Analysis of the Structure and Properties of Expanded Graphite-Filled Poly(phenylene ether)/Atactic Polystyrene Nanocomposite Fibers

Ceyhan Celik,* Steven B. Warner

Materials and Textiles Department, College of Engineering, University of Massachusetts–Dartmouth, 285 Old Westport Road, North Dartmouth, Massachusetts 02747

Received 8 August 2005; accepted 9 November 2005
DOI 10.1002/app.23772
Published online in Wiley InterScience (www.interscience.wiley.com).

ABSTRACT: A miscible blend of 85.5 wt % atactic polystyrene and 9.5 wt % poly(phenylene ether) containing 5.0 wt % expanded graphite nanoparticles was melt-spun and stretched up to 25 times. The structure and electrical and mechanical properties of the fibers were investigated. Characterized by a Hermans orientation factor of 0.6, the nanographite platelets were moderately aligned with the fiber axis, which likely occurred when the polymer itself was partially aligned during drawdown. The electrical conductivity of the oriented filaments was about 10^{-4} S/cm, about what other researchers have measured in comparable unoriented systems. The conductive network of agglomerated graphite nanoparticles did not collapse during drawdown, which led to small protrusions, or bumps, on the fiber surface. The obvious lack of polymer–particle bonding led to reduced extrinsic mechanical properties; both the tensile strength and elongation of the fibers were 20–25% less than those of the neat fibers. The modulus of the oriented fiber was unchanged by the addition of the graphite nanoparticles. © 2006 Wiley Periodicals, Inc. J Appl Polym Sci 103: 645–652, 2007

Key words: conducting polymers; fibers; morphology; nanoparticles; polystyrene

INTRODUCTION

The electrical properties of composites consisting of an insulating matrix and dispersed conducting particles have been extensively studied over the past few decades. Recently, expanded graphite/polymer electrically conductive nanocomposites have attracted great interest.[1] Expanded graphite particles have been combined with polymers such as polystyrene (PS), polyethylene, poly(methyl methacrylate), and polypropylene to prepare electrically conductive nanocomposites.[2,3] A matrix of an aromatic polymer, such as PS or poly(ethylene terephthalate), may to some degree enhance the electrical conduction by the graphite particles contributions from the delocalized electrons in the aromatic rings.[4] PS can be blended with a polymer called poly(phenylene ether) (PPE) to give a miscible blend. PPE is a heat-resistant polymer with a glass-transition temperature (T_g) of about 210°C. Because PS has a T_g of only about 100°C, through the variation of the PS/PPE ratio in the blend, the T_g of the alloy can be increased.[5] Also, the elongation at break and toughness of the blend can be improved.[5]

PS/PPE/expanded graphite nanocomposites can be produced in filament form. In PPE/PS blends, increasing the PPE content increases the viscosity.[6] With the consideration that the addition of 5 wt % expanded graphite can also increase the melt viscosity of the polymer blend,[7] we prepared a polymer blend having a 10/90 weight ratio of PPE to PS. Textile fibers are usually semicrystalline, but we reasoned that the particles could act as crystallites, and the lack of crystal–noncrystalline boundaries was viewed as positive for enhanced electrical conductivity. In addition, we selected about the largest particles we thought we could incorporate into fibers without totally destroying the mechanical properties with an eye toward elevating the electrical conductivity as much as possible. If the particles were to align with their *c* axis, normal to the fiber axis, the reduction in effective cross-sectional area would be minimal.

Like in nylon/montmorillonite composites,[8] particle orientation along the filament axis could be accomplished by a high drawdown, with postdrawing of the filaments, or both. Because postdrawing processes rely on plastic deformation in the filament, we elected to use drawdown only. Studies on the dependence of electrical conductivity on the draw ratios of nanocomposite films and fibers[9,10] have shown that

Correspondence to: S. B. Warner (swarner@umassd.edu).
**Present address:* Saint-Gobain High Performance Materials, Northboro R&D Center, Northboro, MA 01532.

Contract grant sponsor: National Textile Center; contract grant number: M00-MD08.

plastic deformation collapses and breaks the particle network and, therefore, decreases the electrical conductivity of the material. The melt drawdown process relies not on plastic deformation; rather, it uses viscous flow deformation to elongate and attenuate the polymer.[11] With melt drawdown alone, we set out to produce oriented nanocomposite filaments and to minimize the destruction of the particle network. The alignment of high-aspect-ratio expanded graphite particles along the filament axis contributed to the electrical conductivity of the composite by allowing relatively large free-path lengths for electrons with minimal polymer junctions to cross.

EXPERIMENTAL

Materials and processing

Asbury Carbons (Asbury, NJ) kindly supplied thermally expanded graphite flakes (20 and 60 mesh). The PPE/PS (50/50 wt %) blend was supplied by GE Plastics (Pittsfield, MA) as Noryl PKN4717. The weight-average molecular weight of the PS was 280,000 g/mol, and that of the PPE was 25,000 g/mol. Atactic PS with a weight-average molecular weight of 245,000 g/mol was supplied by Nova Chemicals (Alberta, Canada) as PS 2500. American Chemical Society certified ethyl alcohol and toluene were purchased from Fisher Scientific (Hampton, NH).

Expanded graphite flakes were wet ball-milled for 96 h in the presence of ethyl alcohol to obtain graphite particles having large dimensions of a few micrometers and less.[3] The slurry was screened with sieves with a 35 μm pore opening and dried in a hood at 60–65°C for 12 h and then in a vacuum oven at 150°C for 12 h. Last, we dry-ball-milled the particles for an additional 96 h in hope of further reducing the particle size and breaking particle agglomerations.

Solution blending was used because it seemed unlikely that in a relatively short-barrel-length ($\sim$ 50 cm) single-screw extruder, sufficient shear would be generated in the melt to break particle agglomerates and adequately disperse the nanoparticles. PS (30 g) and PPE/PS (50/50 wt %; 8 g) were dissolved at room temperature in 300 mL of toluene with the aid of mechanical stirring. Expanded graphite (2 g) was dispersed in 100 mL of toluene with a sonicator for 30 min. The mixture was added dropwise to the polymer/toluene solution as mechanical stirring continued. Homogeneity was achieved with a mechanical stirrer and a sonicator for 1 h, whereas hot air was directed onto the solution surface from an air blower to hasten solvent evaporation. The solution was left drying overnight in the hood and postdried in a vacuum oven at 150°C for 24 h; this was designed to remove any remaining toluene.

Melts were extruded through a dye (diameter = 0.4 mm) with a Brabender IntelliTorque single-screw extruder (Hackensack, NJ) with three heating zones. Polymeric composite material was gravity fed into zone 1 of the extruder. Heating zones were set to 250, 257, and 265°C, respectively. Monofilaments were collected with a Randcastle RCP monofilament winding machine (Cedar Grove, NJ), which was placed below the extruder die. The distance between the extruder die and the take-up point was 75 cm. Filament drawdown was as high as 35 : 1.

Characterization and measurements

Birefringence

The retardance of as-spun fibers was assessed with a Leitz DMR polarized light microscope (Wetzlar, Germany). Filaments were immersed in Cargille refractive index liquid (n = 1.592) and were observed on their side in polarized light. The retardance of the neat and nanocomposite filaments was obtained with a Leica four-order tilting compensator (Wetzlar, Germany). The birefringence, retardance divided by diameter, values reported are based on an average of retardance measurements taken for six individual filaments. The same microscope was used to determine the monofilament diameter with a calibrated filar micrometer eyepiece and a Boeckeler Microcode II digital readout (Tucson, AZ). Three readings per sample were taken, and an average value was used in birefringence calculations.

Density

Filament density measurement by a gradient tube according to ASTM 1505 was conducted by Advanced Plastics and Material Testing (Ithaca, NY). The column contained water and calcium nitrate, which gave a density range of 1.000–1.600 g/cm^3. Column sensitivity was 0.0001 g cm^{-3} mm^{-1}. Six replications were conducted on each sample.

Differential scanning calorimetry (DSC)

Samples sealed in aluminum pans were probed under nitrogen flow with a TA Instruments Q1000 differential scanning calorimeter (New Castle, DE). Data were obtained with a heat–cool–heat cycle between −50 and 270°C at a linear heating rate of 20°C/min and a linear cooling rate of 10°C/min. Results were analyzed with TA Universal Analysis software.

Scanning electron microscopy (SEM)

For the SEM observation, samples were placed onto an aluminum stub covered with double-sided sticky

carbon tape and plated with gold with a Denton Vacuum Desk II sputtering machine (Moorestown, NJ). A JEOL JSM-5610 high-vacuum scanning electron microscope (Tokyo, Japan) was used to study ball-milled graphite particles, freeze-fractured and Instron-fractured filament cross-sections, and filament surfaces.

Particle size analysis

Examination of the ball-milled graphite particles with SEM suggested their thickness was on the order of 100 nm, which was consistent with the manufacturer's specification. The specific surface area of the ball-milled particles was determined with nitrogen adsoprtion in a Quantichrome Nova model e-1000 Brunauer-Emmett-Teller (BET) analyzer (Boynton Beach, FL). Assuming the graphite nanoparticles were platelike, we were able to calculate an average plate diameter; the results were consistent with SEM observations.

Wide-angle X-ray diffraction

Wide-angle X-ray diffraction experiments were conducted at the Center for Materials Science and Engineering at the Massachusetts Institute of Technology. Graphite powder and nanocomposite filaments were examined, and (002) diffraction data from the graphite particles were gathered with a Rigaku RU 300 (Tokyo, Japan) and a Bruker AXS Smart Apex goniometer (Madison, WI). Cu Kα radiation at 60 kV and 300 mA was used. The intensity data were obtained in a 2θ range of 5 to 80°.

Tensile testing

Tensile modulus, strength, and elongation at break were measured with an Instron model 5569 mechanical testing machine (Canton, MA). The gage length was set at 2.54 cm, and the strain rate was 10%/min. Twenty monofilaments were tested for each experiment. Before testing, each monofilament's diameter was measured with the optical microscope technique described previously for birefringence.

Electrical conductivity

ASTM D 257, the most widely accepted test for determining conductivity of plastics, was followed to determine the electrical conductivity. Filaments were cut to 1 cm lengths, their ends were embedded in silver paint, and they were vacuum-dried at 105°C for 24. Volume conductivity was measured with a Mahlo DMB 10 high-resistance measurement instrument (Saal/Donqu, Germany) while samples rested on a polycarbonate sheet.

RESULTS AND DISCUSSION

The birefringence of both the nanocomposite and neat filaments obtained at a 25 : 1 drawdown was approximately −0.005. Uchiyama and Yatabe[12] studied the birefringence of uniaxially oriented poly(para phenylene oxide) (PPO/PS) blends. Their birefringence measurements of 10/90 wt % PPO/PS films, which were drawn 200%, was also approximately −0.005; hence, our results are consistent with those of Uchiyama and Yatabe.[12]

Negative birefringence develops in PS as molecular orientation along the filament axis and increases with take-up velocity. Uchiyama and Yatabe[12] referenced the intrinsic birefringence of PS and PPO films at 486 nm, determined by dichroic IR measurements and optical birefringence by Lefebvre et al.[13] According to Lefebvre et al., the intrinsic birefringences of PS and PPO (films) at 486 nm are −0.10 and 0.21. We used the following equation to estimate the intrinsic birefringence of the 10/90 wt % PPE/PS. Although we had a solution, not a mixture, the following equation was adequate for obtaining an estimate of birefringence (Δn):

$$\Delta n = \sum_i V_i \Delta n_i + \Delta n_f \quad (1)$$

where i is the ith component, V_i is the volume fraction, Δn_i is the intrinsic birefringence of the component polymer, and Δn_f is the form birefringence. Because the blends were compatible,[12] form birefringence should have been negligibly small in the PPE/PS blends. The intrinsic birefringence of 10/90 wt % PPE/PS was estimated to be −0.066. Comparing the estimated birefringence of the blend to the birefringence of the nanocomposite and neat filaments obtained at 25 : 1 drawdown, we deduced that the molecules were oriented but not highly oriented. The presence of expanded graphite did not change the birefringence of PPE/PS. The results support the assumption that form birefringence was negligible.

SEM

SEM photomicrographs of the mating fracture surfaces of a composite filament drawn down 25 : 1 taken after mechanical testing are shown in Figure 1. Graphite nanoparticles appeared to be unattached to the polymer matrix and the nanoparticle surfaces were often free of polymer, which suggested poor polymer–particle interaction in the composite. As shown in Figure 1, some voids surrounded the particles; however, density measurements that appear

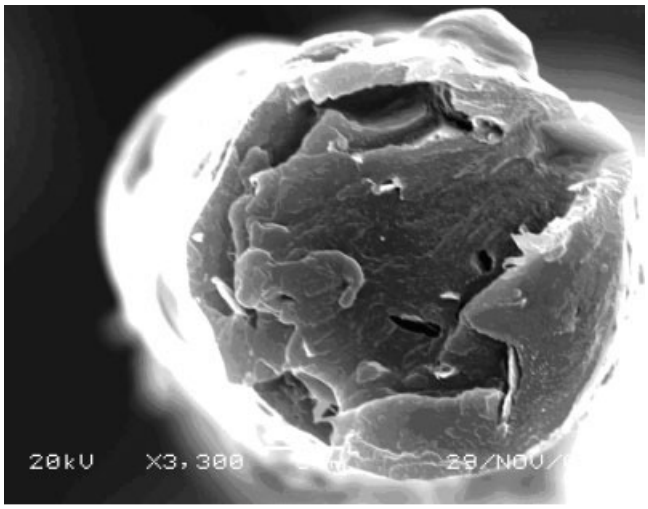

(a)

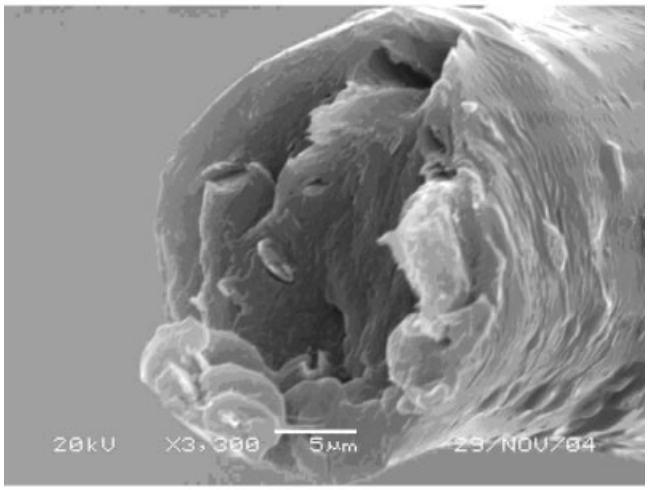

(b)

Figure 1 SEM images of the mating tensile fracture surfaces of the expanded graphite/PPE/PS nanocomposite filament after 25 : 1 drawdown.

later in the results suggested a near void-free composite. Hence, it seemed likely that the void was created by debonding during mechanical deformation. On the other hand, some particles, especially the larger ones, seemed to be surrounded by polymer. We envisioned that the high-viscosity polymer matrix encompassed the particles. Sometimes, the fracture occurred at the interface; sometimes, the fracture surface skirted the particles. Skirting was not necessarily evidence for polymer–particle bonding.

As shown in Figure 2, the surface of the nanocomposite filaments were bumpy, whereas filaments made from the polymer blends were smooth surfaced. As the nanoparticle content reached toward the threshold of forming a network, some large agglomerates apparently created hemispherical-like polymer structures on the polymer surface.[14] During filament drawdown between fiber-die and take-up, the fiber diameter decreased, but the solid particle network resisted. Thus, the expanded graphite particles that were both part of the network and close to the thinning filaments' surface led to the appearance of polymer-coated knobs protruding from the surface.

BET measurements showed a specific surface area of about 38 m^2/g. With a platelet thickness of 100 nm, we calculated an average plate diameter of 12 μm. With SEM, we saw some large platelets, perhaps double this dimension, and platelets smaller than 1 μm in diameter.

Density

The density of 10/90 wt % PPE/PS was calculated with eq. (2) to be 1.05 g/cm^3, which was for mixtures; however, it was sufficiently accurate for obtaining an estimate:

$$\rho_{\text{PPE/PS (10/90)}} = \rho_{\text{PS}} V_{\text{PS}} + \rho_{\text{PPE/PS (50/50)}}(1 - V_{\text{PS}}) \quad (2)$$

where $\rho_{\text{PPE/PS (10/90)}}$ is the density of 10/90 wt % PPE/PS, ρ_{PS} is the density of 100% PS, $\rho_{\text{PPE/PS (50/50)}}$ is the density of 50/50 wt % PPE/PS, and V_{PS} is the volume fraction of 100% PS.

We also calculated the polymer, or matrix, density (ρ_m) of the nanocomposite filaments by subtracting the part due to graphite from the measured filament density (ρ_f) according to the following formula:[15]

$$\rho_m = \frac{\rho_f - \rho_g \times V_g}{V_m} \quad (3)$$

where ρ_g is the graphite density (2.25 g/cm^3) and V_g and V_m are the volume fractions of graphite and matrix.

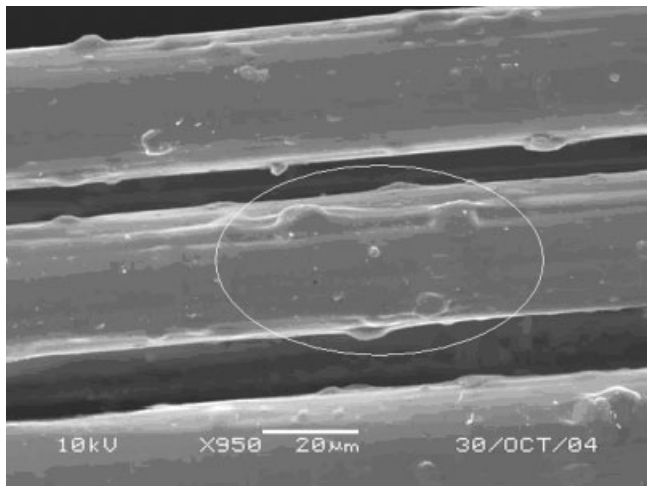

Figure 2 SEM image of nanocomposite filament surfaces after 25 : 1 drawdown, showing surface protrusions.

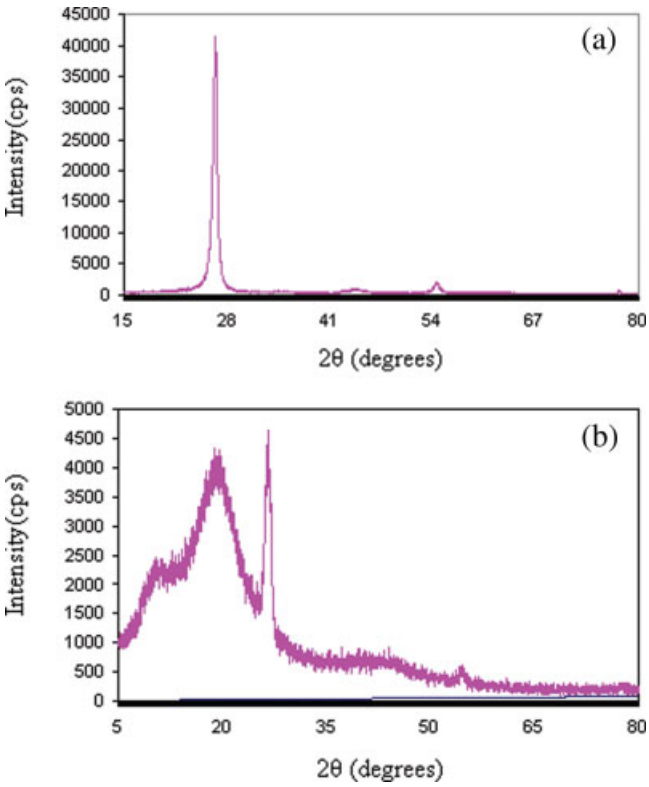

Figure 3 X-ray powder diffraction patterns of (a) expanded graphite and (b) the expanded graphite/PPE/PS nanocomposite filaments. [Color figure can be viewed in the online issue, which is available at www.interscience.wiley.com.]

The measured density of neat filaments obtained after a 35 : 1 drawdown was 1.07 g/cm^3. We attributed the high filament density to the molecular orientation of the amorphous polymer, that is, due to closer packing of polymer chains in oriented material.[11,14] The measured density of the nanocomposite filaments obtained after a 25 : 1 drawdown was also 1.07 g/cm^3.

The matrix density of the nanocomposite filaments was calculated to be 1.05 g/cm^3. The matrix density of nanocomposite filaments obtained at a 25 : 1 drawdown was, as expected, lower than that of neat filaments obtained at a 35 : 1 drawdown. Also, during drawdown, the expanded graphite particles might have hindered the alignment of the polymer chains along the filament axis. Another reason for the relatively low nanocomposite matrix density might have been defects and small voids, which could have been created by the inclusion of expanded graphite particles or at very high drawdown. The weak van der Waals interaction between expanded graphite particles and polymer perhaps led to the development of defects and voids during fiber drawdown, even before Instron testing. Large voids were present in the SEM images shown in Figure 1 on deformed fibers. The deformation process likely enhanced void size, but small voids might have been present in the as-made fiber.

X-ray diffraction

Shown in Figure 3 are the X-ray diffraction patterns of expanded graphite and PPE/PS/expanded graphite nanocomposite filaments. Diffraction from (002) was observed at $2\theta = 26.518$ and 26.289°. The (002) graphite diffraction peak was also strong in the nanocomposite filaments. PS showed broad features near $2\theta = 10$ and 18°.[16] In 10/90 wt % PPE/PS neat and composite filaments, broad features near $2\theta = 10$ and 19° were observed. The shift from 18 to 19° could be explained with the following statement:

> The assumption of a constant azimuthal location of the amorphous scattering does not work perfectly for drawn fibers. It is necessary to consider a shift toward larger angles of the amorphous scattering on the equator, which means that the amorphous chains oriented parallel to the draw axis and more densely packed than the less oriented ones but not always taken into account by Murthy et al.[17]

Hermans orientation function was used to evaluate particle orientation:

$$P = \frac{3\left(\cos^2 \psi\right) - 1}{2} \tag{4}$$

where P is Hermans orientation factor and ψ is the full width at half-maximum of the azimuthal scan.

Full width at half-maximum of the (002), obtained from an X-ray diffraction photograph taken of a bundle

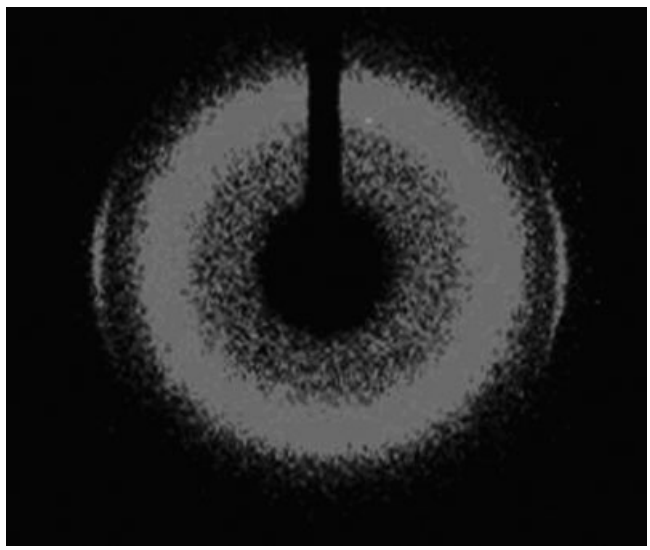

Figure 4 Two-dimensional X-ray diffraction pattern of expanded the graphite/PPE/PS filament bundle obtained after 25 : 1 drawdown. The fiber orientation was vertical.

TABLE I
Mechanical Property Data for the Neat and Composite Filaments

Material	Drawdown	Filament diameter (μm)	Modulus (MPa)	Standard deviation	Tensile strength (MPa)	Standard deviation	Elongation at break (%)	Standard deviation
Neat filament	5 : 1	308	3030	116	56	3	4.01	0.87
	25 : 1	47	4207	227	74	4	2.12	0.24
	35 : 1	22	5028	275	102	11	2.00	0.18
Composite filament	5 : 1	289	3241	122	44	8	3.06	0.75
	25 : 1	50	4112	135	64	9	1.99	0.17

of parallel nanocomposite fibers drawn down 25 : 1 and shown in Figure 4, was measured to be 31°. Hermans orientation factor for the expanded graphite nanoparticles was 0.6, which is consistent with the notion that the graphite platelets are generally aligned along the filament axis, presumably due chiefly to polymer flow patterns.

Loo and Gleason[8] determined the orientation distribution of montmorillonite clay in nylon 6 nanocomposite films with a combination of IR trichroic analysis and transmission electron microscopy image analysis. They described the montmorillonite clay orientation in spun-cast nylon 6 films with a Gaussian function having a standard deviation of 15°. They reported that 95% of the clay platelets were tilted at an angle of not more than ±30° out of the plane of the film. Thus, the extent of expanded graphite platelet alignment along our most highly oriented filaments (25:1 drawdown) was comparable to the alignment of the montmorillonite in nylon 6 nanocomposite films reported by Loo and Gleason.[8]

Mechanical properties

Mechanical testing results revealed that the Young's modulus of the nanocomposite filaments was not significantly different from that of the neat polymer filaments produced at the same drawdown. However, the Young's modulus of all filaments showed a significant increase with increasing drawdown, which as expected, induced polymer and particle orientation along the filament axis. The average modulus values are shown in Table I. The mechanical properties of a particle-reinforced nanocomposite depend on the bonding between the particle and the matrix.[18] Because the volume fraction of expanded graphite particles was relatively low and particle–polymer bonding was only weak van der Waals forces, the expanded graphite particles did not contribute to the Young's modulus of the filaments.

The average tensile strength and elongation at break of the neat and nanocomposite filaments obtained from 20 measurements are given in Table I. The tensile strength of the nanocomposite filaments decreased up to 20% with the addition of 5 wt % expanded graphite. This strength loss could be explained by the fact that particles were essentially unbonded and acted like voids, like defects. Also contributing were poor particle dispersion, the presence of some very large particles that effectively reduced the load-bearing cross-sectional area of the filaments, and nonaxial molecular orientation in the vicinity of the large particles.

The elongation at break of both neat and composite filaments, of course, decreased with increasing drawdown; however, the elongation at break of the composite filaments was up to 24% less than that of the corresponding neat filament. The elongation at break values showed that these fibers were glassy and brittle.

All in all, the decrease in mechanical properties was disappointing but not wholly unexpected. Our goal was to achieve high conductivity. Perhaps a better approach would be to surface-treat the particles in such as was that they bond to the matrix yet do not suffer from increased contact resistivity.

Electrical resistivity

The electrical resistivity results of the PPE/PS nanocomposite filaments containing expanded graphite are given in Table II. The electrical resistivity of the nanocomposite filaments obtained at 5 : 1 and 25 : 1 drawdowns did not show a significant difference, and the average volume resistivity of the nanocomposite filaments was approximately 10^4 Ω cm, clearly all in the range of a semiconductor. The results show that expanded graphite platelets were effective at decreasing the polymer fiber's resistivity at low particle concentration. Neat PS has a resistivity of approximately 10^{16} Ω cm, and neat PPE has a resistivity of approximately 10^{17} Ω cm.[5]

TABLE II
Average Electrical Resistivity of the Nanocomposite Filaments

Drawdown	5 : 1	25 : 1
Average electrical resistivity (Ω cm)	2×10^4	1.3×10^4
Standard deviation	1.7×10^4	1×10^4

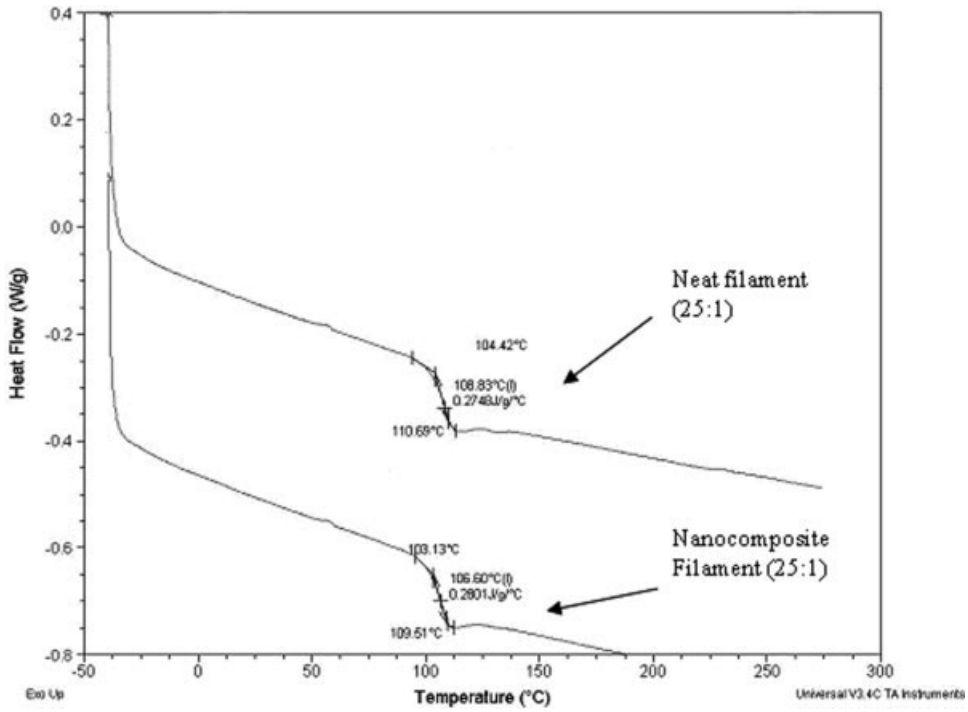

Figure 5 DSC curves of neat PPE/PS and the nanocomposite filaments obtained after 25 : 1 drawdown.

In our nanocomposite filaments, the alignment of the particles along the fiber axis allowed a longer free path for electron transport, and fewer places that the electrons needed to pass through the polymer than is the case for randomly oriented platelet-shaped particles. The properties that influence the conductivity of conductive particle-filled polymeric composite materials are particle shape, size, aspect ratio, orientation, and polymer conductivity.[8] The electrical resistivity of samples containing drawn polymer loaded with carbon black typically deteriorates as the particles separate and voids form.[9]

In a previous study, Chen et al.[3] reported that at a concentration of 5 wt %, the electrical resistivity of expanded graphite/PS bulk nanocomposites (not fibers) was 10^2 Ω cm. In another study, also on the electrical resistivity of bulk samples, Fukushima and Drzal[2] reported a resistivity of 10^3 Ω cm at 5 wt % expanded graphite concentration. Both values are lower than those we obtained on oriented fibers, but all the results show a similar result: a decrease of more than 10 orders of magnitude in resistivity with the addition of about 5 wt % nanographite. Unfortunately, the orientation of the nanoparticles did not appear to improve the conductivity above that of unoriented material, which suggested that the connectivity of the particles is key.

TABLE III
T_g of the Polymers or Fibers of the Neat PS, PPE/PS, and Nanocomposite

Material	T_g (°C)
PS	100
PPE	210
PPE/PS filament (25 : 1)	108
Nanocomposite filament (25 : 1)	107

DSC

The thermal behavior of the neat and nanocomposite filaments is shown in Figure 5. The T_g values of PS, PPE, 10/90 wt % PPE/PS, and the nanocomposite material are compiled in Table III.

The neat and nanocomposite polymer fibers had very similar DSC traces. As shown in Table III, the measured T_g values of both the neat PPE/PS filaments and expanded graphite–PPE/PS filaments obtained after a 25 : 1 drawdown were about 107°C, which was almost 8°C higher than the T_g of PS. This difference was due to the presence of PPE, which has stiff polymer chains. The presence of expanded graphite platelets did not significantly elevate the T_g of PPE/PS polymer system, an observation that was consistent with the lack of a strong bond between polymer chains and particles.

CONCLUSIONS

Nanocomposite filaments with diameters as low as 30 μm were produced by melt-spinning. Because of the low PPE content and the presence of unmodified expanded graphite particles, the filaments were glassy and brittle. Elongational polymer flow did not

collapse the graphite nanoparticle networks. Therefore, some of the expanded graphite platelets and agglomerates created a bumpy fiber surface, which appeared as small knobs on the fibers. In contrast, the neat filament surface was relatively smooth. The continuous graphite particle network improved the electrical conductivity. The birefringence of the nanocomposite and neat filaments obtained at a 25 : 1 drawdown was approximately −0.005, which could be usefully compared to the estimated intrinsic birefringence of the blend, −0.066. The orientation of polymer chains increased the neat filaments' density from 1.05 to 1.07 g/cm^3, likely because of denser packing of polymer chains.[14] The orientation of the polymer molecules was responsible for the increase in Young's modulus. The neat filaments' Young's modulus increased up to 70% with increasing drawdown; however, the addition of 5 wt % expanded graphite did not significantly affect the modulus. The average volume resistivity of the nanocomposite filaments obtained at 5:1 and 25:1 drawdowns was approximately 10^4 Ω cm. The alignment of the graphite platelets along the filament axis was effected by drawdown and created a longer path for easy electron transport; however, the electrical conductivity was no greater than that typically seen in comparable unoriented samples. Particle–particle contact seemed to chiefly determine the conductivity of the polymer loaded with conductive nanographite. From particle network formation and observations of bulging on the surface, we had undeniable evidence that particles agglomerated. The expanded graphite platelets and agglomerates were mechanical defects in the resin polymer and decreased the tensile strength up to 20% and the elongation at break up to 24%. The addition of expanded graphite particles did not significantly elevate the T_g of the PPE/PS polymer system, which was consistent with the lack of a strong bond between the polymer chains and particles.

The assistance of Skander Limen and Esin Yesilalan in obtaining the SEM images is appreciated.

References

1. Chen, X.; Shen, J.; Huang, W. J Mater Sci Lett 2002, 21, 213.
2. Fukushima, H.; Drzal, L. T. Soc Plast Eng Annu Tech Conf Compos Div 2003, 2230.
3. Chen, G.; Wu, D.; Weng, W.; Yan, W. J Appl Polym Sci 2001, 82, 2506.
4. Nalwa, H. S. Handbook of Organic Conductive Molecules and Polymers; Wiley: New York, 1997.
5. Industrial Polymers Handbook Products, Processes, Applications; Edward, S. W., Ed.; Wiley-VCH: New York, 2001; Vol. 3.
6. Rodriguez, F.; Cohen, C.; Ober, C. K.; Archer, L. A. Principles of Polymer Systems, 5th ed.; Taylor & Francis: New York, 2003.
7. Shah, R. K.; Paul, D. R. Polymer 2004, 45, 2991.
8. Loo, L. S.; Gleason, K. K. Polymer 2004, 45, 5933.
9. Hirofumi, Y.; Toshiyuki, K. Sen'i Gakkaishi 2004, 60, 365.
10. Hoon, K. S.; Min, B. G.; Lee, S. C.; Park, S. B.; Lee, T. D.; Park, M.; Kumar, S. Fibers Polym 2004, 5, 198.
11. Ziabicki, A.; Kawai, H. High-Speed Fiber Spinning, Science and Engineering Aspects; Wiley: New York, 1985.
12. Uchiyama, A.; Yatabe, T. Jpn J Appl Phys 2003, 42, 3503.
13. Lefebvre, P.; Jasse, B.; Monnerie, L. Polym 1982, 23, 706.
14. Chen, X.; You, B.; Zhou, S.; Wu, L. Surf Interface Anal 2003, 35, 369.
15. Giza, E.; Ito, H.; Kikutani, T.; Okui, N. J Macromol Sci Phys 2000, 39, 4, 545.
16. Fawn, M. U.; Wilkie, C. A. Polym Degrad Stab 2002, 76, 111.
17. Ibanes, C.; David, L.; Seguela, R.; Vigier, G.; Boissieu, M. D.; Robert, G. Polym Mater Sci Eng 2002, 86, 283.
18. Lordi, V.; Yao, N. J Mater Res 2000, 15, 12.